Non-Gaussian power grid frequency fluctuations characterized by Lévy-stable laws and superstatistics

Benjamin Schäfer [1,2]*, Christian Beck[3], Kazuyuki Aihara [4], Dirk Witthaut [5,6] and Marc Timme[1,2]

Multiple types of fluctuations impact the collective dynamics of power grids and thus challenge their robust operation. Fluctuations result from processes as different as dynamically changing demands, energy trading and an increasing share of renewable power feed-in. Here we analyse principles underlying the dynamics and statistics of power grid frequency fluctuations. Considering frequency time series for a range of power grids, including grids in North America, Japan and Europe, we find a strong deviation from Gaussianity best described as Lévy-stable and q-Gaussian distributions. We present a coarse framework to analytically characterize the impact of arbitrary noise distributions, as well as a superstatistical approach that systematically interprets heavy tails and skewed distributions. We identify energy trading as a substantial contribution to today's frequency fluctuations and effective damping of the grid as a controlling factor enabling reduction of fluctuation risks, with enhanced effects for small power grids.

The Paris Conference in 2015 set a path to limit climate change "well below 2 °C"[1]. To reach this goal, integrating renewable and sustainable energy sources into the electrical power grid is essential[2]. Wind and solar power are the most promising contributors to reach a sustainable energy supply[3,4], but their integration into the existing electric power system remains an enormous challenge[5–7]. In particular, their power generation varies on all timescales from several days[8] to less than a second[9], displaying highly non-Gaussian fluctuations[10]. This variability must be balanced by storage facilities and back-up plants, requiring precise control of the electric power grid.

The central observable in power grid monitoring, operation and control is the grid frequency f (ref. [11]). In the case of excess demand, kinetic energy of large synchronous generators is converted to electric energy, thereby decreasing the frequency. Dedicated power plants measure this decrease and increase their generation to stabilize the grid frequency within seconds to minutes (primary control)[11,12]. On longer timescales, additional power plants are activated to restore the nominal grid frequency (secondary control). The increase of renewable generation challenges this central control paradigm, as generation becomes more volatile and the spinning reserve decreases[13]. How to provide additional effective/virtual inertia is under intensive development[14,15]. In addition, fluctuating demand[16] and fixed trading intervals[17] already contribute to frequency deviations.

A detailed understanding of the fluctuations of power grid frequency essentially underlies the design of effective control strategies for future grids. Many studies for simplicity assume Gaussian noise[16,18–21], while non-Gaussian effects are only rarely studied[22–25]. Gaussian approaches neglect the possibility of heavy tails in the frequency distributions and thus strong deviations from the reference frequency, posing serious contingencies particularly relevant for security assessment. Even in studies considering non-Gaussian effects, the connection to real data is missing[22], realistic but isolated wind and solar data are only numerically evaluated[24,25] or the focus is on static power dispatch[16,21,23] as opposed to real-time dynamics.

It is crucial to understand how collective grid dynamics are driven by the fluctuations originating from varying power demands, fluctuating input generation and trading. While realistic models describing the actual noise input of wind and solar power exist[24,25], the impact of fluctuations on grid dynamics has been studied for selected specific scenarios, regions or technologies only[26,27]. Furthermore, a systematic quantitative comparison of different sized synchronous regions based on their frequency fluctuations is needed. It is important to forecast fluctuation statistics in grids of any size, especially when setting up small isolated systems, for example on islands or disconnected microgrids[28].

In this Article, we analyse the frequency fluctuations observed in several electric power grids from three continents. We determine and characterize the non-Gaussian nature of these fluctuations existing across grids in both the 60 Hz and 50 Hz operation regimes. Furthermore, we propose an analytically accessible model that successfully describes these data in one consistent framework by systematically incorporating the non-Gaussian nature of fluctuations, and verify its predictions. The analysis yields trading as a key factor for non-Gaussianity. Extracting the effective damping for different synchronous regions via autocorrelation measures, our work highlights that the effective grid damping as well as the size of the grid itself serve as controlling factors to make grid dynamics more robust. Finally, we demonstrate how superstatistics explains heavy tails and skewness using superimposed Gaussian distributions.

[1]Chair for Network Dynamics, cfaed and Institute for Theoretical Physics, Technical University of Dresden, Dresden, Germany. [2]Network Dynamics, MPIDS, Göttingen, Germany. [3]School of Mathematical Sciences, Queen Mary University of London, London, UK. [4]Institute of Industrial Science, The University of Tokyo, Meguro-ku, Tokyo, Japan. [5]Forschungszentrum Jülich, Institute of Energy and Climate Research-Systems Analysis and Technology Evaluation, Jülich, Germany. [6]Institute for Theoretical Physics, University of Cologne, Köln, Germany. Dirk Witthaut and Marc Timme contributed equally to this work. *e-mail: benjamin.schaefer@ds.mpg.de
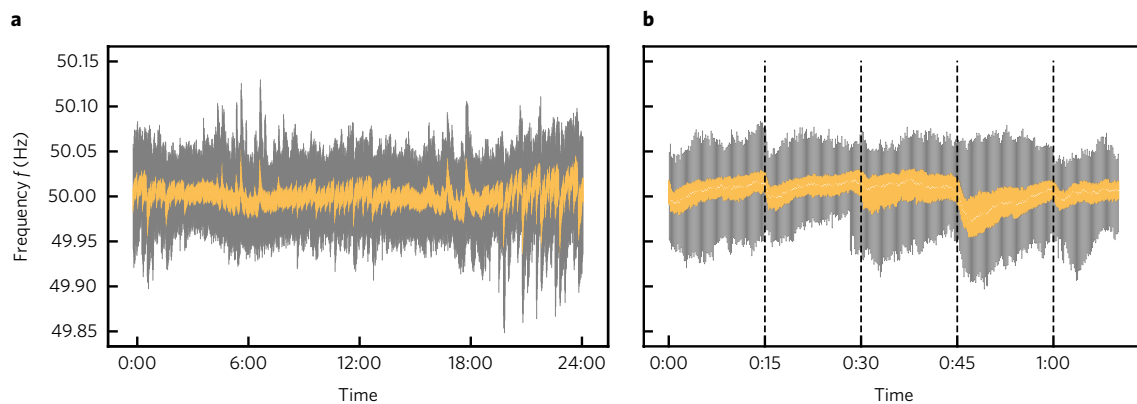
Fig. 1 | Fluctuations in frequency around the reference frequency of 50 Hz. a, Box plot of the 2015 data by Réseau de Transport d'Electricité (RTE)[29] describing the CE power grid. **b**, Zoom-in on the first 70 min of the frequency measurements, exposing substantial changes in average and variance of frequencies at 15 min trading intervals (indicated by the dashed lines). Each box contains data of one year for the same time instance (averaged per minute in **a**). The yellow bars contain the 25% and 75% quartiles; the grey bars are the whiskers giving the maximum and minimum values and the white line is the median value.

Observing the statistics of frequency fluctuations. The bulk frequency of a power grid fluctuates around its nominal frequency of 60 Hz (most parts of America, western Japan, Korea, Philippines) or 50 Hz (eastern Japan and other countries). To understand and quantify these fluctuations, we analyse datasets for the power grid frequency of the European Network of Transmission System Operators for Electricity (ENTSO-E) Continental European (CE)[29,30], Nordic[31], Mallorcan[32] and Great Britain (GB)[33] grids, the 50 Hz and 60 Hz regions of Japan[34] and the Eastern Interconnection (EI) in North America[35], see Supplementary Note 1 for more detailed data breakdown. The data consist of power grid frequency measurements at one location in the given region (two for CE) at a sampling rate between ten measurements per second and one measurement per five minutes.
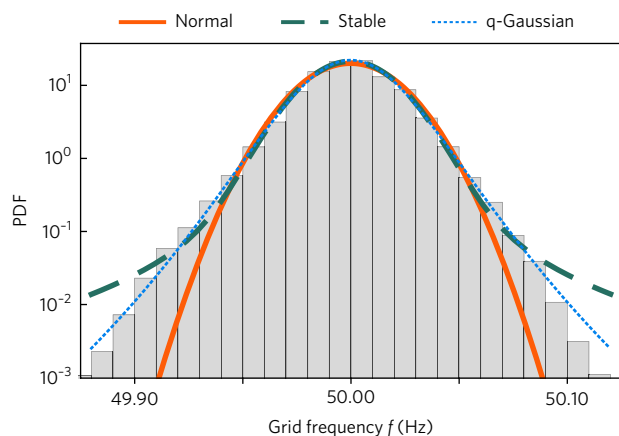

Fig. 2 | Non-Gaussian nature of the frequency distribution. The 2015 dataset by 50Hertz describing the CE power grid, where fitted normal, stable and q-Gaussian distributions are compared with the histogram data using a log scale for the probability density function (PDF). Deviations from a normal distribution become evident in the tails, which are more pronounced than expected for a normal distribution. The stability parameter of the stable distribution is $\alpha_S = 1.898 \pm 0.002$ and the deformation parameter of the q-Gaussian distribution is $q = 1.20 \pm 0.01$, whereas $\alpha_S^{Gauss} = 2$ and $q^{Gauss} = 1$ for Gaussian distributions. The Lévy-stable distribution uses four fitting parameters, while the q-Gaussian uses three and the normal distribution uses two parameters.

At first glance, a typical recording of the grid frequency (Fig. 1) reveals that it coincides extremely well with the nominal grid reference frequency, highlighting the efficiency of today's frequency control. Only rarely do we observe large deviations from the nominal frequency. These large disturbances often occur when a new power dispatch has been settled on by trading (every 15 min), introducing jumps and fluctuations of the frequency. The total variance of the frequency fluctuations in a given region thereby depends on the size of the grid—larger grids are more inertial and thus tend to have a smaller variance.

All distributions deviate from Gaussian distributions, which becomes evident when observing their tails (Fig. 2). For the CE, Nordic, Mallorcan and Japanese grids large deviations from the nominal frequency are more frequent than for a Gaussian distribution of given variance, leading to heavy tails, as quantified, for instance, by an excess kurtosis; see Methods. The grids of GB and the EI, however, are substantially skewed; that is, they are asymmetric around the reference frequency such that deviations are more likely towards lower frequencies than towards higher ones.

Lévy-stable[36] and q-Gaussian distributions[37] are the best fitting distributions among all distributions tested, as identified by a maximum likelihood analysis; see Fig. 2 and Supplementary Note 1. Both distributions generalize a Gaussian distribution to include heavy tails and point to two different microscopic mechanisms underlying the frequency dynamics: q-Gaussians arise when the power fluctuations are Gaussian on short timescales, but with a variance or mean changing on longer timescales. In contrast, Lévy-stable distributions arise when the underlying power fluctuations are heavy tailed or skewed themselves. We investigate both settings in more detail below.

In addition to the aggregated data, we investigate the autocorrelation of the recorded trajectories, extracting important events and the characteristic timescales during which the system decorrelates. Analysing the autocorrelation for the CE grid reveals pronounced correlation peaks every 15 min and especially every 30 and 60 min; see Fig. 3. These regular correlation peaks appear in many grids (CE, GB, Nordic) and are explained by the trading intervals in most electricity markets[17], which are often 30 or 15 min. Furthermore, this is also in line with the observation of large deviations in the frequency trajectories (see Fig. 1), so trading has an important impact on frequency stability. At the beginning of a new trading interval, the production changes nearly instantaneously and the complex dynamical power grid system needs some time to relax to its new operational state.
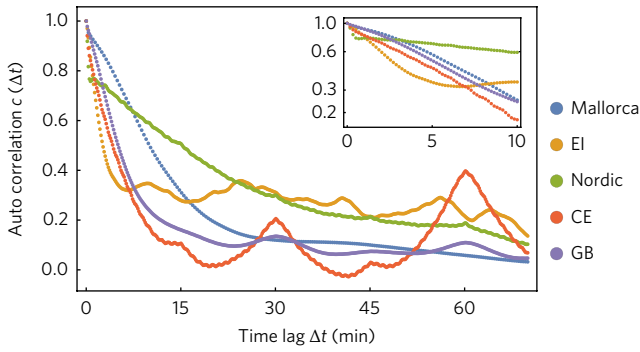
Fig. 3 | Decay of the autocorrelation of the frequency dynamics.
Autocorrelation measures as a function of time lag Δt for the 50Hertz dataset for CE of 2015, the GB grid of 2015, the EI data for one day of 2015, the Nordic grid data of 2015 and Mallorcan data of 2015. After an initial decay of the autocorrelation, peaks emerge every 15 min due to trading intervals; this is especially pronounced for the GB and CE grids, consistent with Fig. 1. Using a log plot in the inset allows extraction of the damping of the grid based on the assumption of exponential decay, equation (1). Note that the CE, GB and EI grids all display similar decays during the initial 5 min. In contrast, the Nordic grid displays a fast decay and then a slower one. The plot uses one full year of frequency data with 1s resolution for each region to generate the autocorrelation plots. The trading peaks in particular are typically not visible when only 24 h of recordings are considered (as for the EI grid).

The decay of the autocorrelation provides further information about the underlying stochastic process. For the first minutes of each trajectory, we observe an exponential decay of the autocorrelation c as a function of the time lag Δt:

$$c(\Delta t) \sim \exp(-\Delta t / \tau), \tag{1}$$

with a typical correlation time τ, as expected for elementary stochastic processes without memory such as the Ornstein–Uhlenbeck process[38].

We extract the inverse correlation time τ^{-1} for each available dataset and obtain values within the same order of magnitude across all grids; see Fig. 4. The Japanese dataset only has measurements every 5 min, hence we refrain from estimating an autocorrelation.
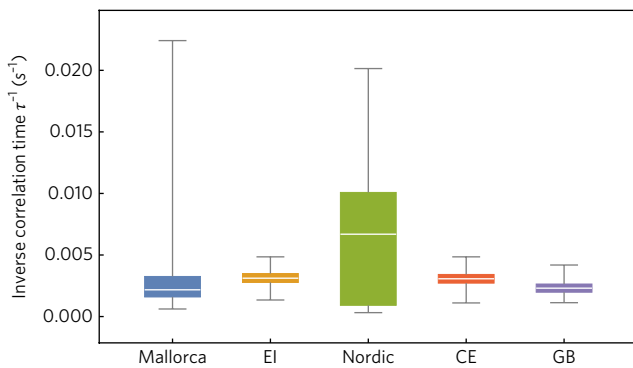

Fig. 4 | Inverse correlation time of different regions. The box plots display the estimate of τ^{-1} based on the autocorrelation decay fitted by an exponential function; see equation (1). The data are obtained by evaluating individual days of all years available and splitting the one day of EI into 10 min trajectories. The box covers the 25% and 75% quartiles, with the white line being the median, while the whiskers give the maximum and minimum values.

The inverse correlation time can be seen as the effective damping γ in a synchronous region with $\gamma := \tau^{-1}$, see below. With this in mind, it is not surprising that all grids return values for γ of the same order of magnitude because the synchronous machines in these regions do not differ substantially. This damping consists of mechanical damping, damper windings and primary control.

Stochastic model of power fluctuations. The variations of the grid frequency are driven by fluctuations of power generation and demand. To link the evolution of the grid frequency with the power injections, we make use of the well established swing equation[11,12,39–44]. Aggregating over the grid, we obtain a Fokker–Planck equation that models the observed frequency fluctuations and allows an analytical description of power grid frequency fluctuations.

We analyse frequency dynamics of a power grid on coarse scales. Every node in the grid corresponds to a large generator (power plant) or a coherent subgroup and is characterized by the phase θ_i and the angular velocity $\omega_i = 2\pi(f_i - f_R)$. Here f_i denotes the frequency of the nodes $i = 1, \ldots, N$ and $f_R = 50$ Hz or $f_R = 60$ Hz is the reference frequency at the grid. The equations of motion of the phase and velocity are then given by

$$
\begin{aligned}
\frac{d}{dt}\theta_i &= \omega_i, \\
M_i \frac{d}{dt}\omega_i &= P_i + \epsilon_i \xi_i - D_i \omega_i + \sum_{j=1}^{N} K_{ij}\sin(\theta_j - \theta_i),
\end{aligned}
\tag{2}
$$

where we have at each node i inertia M_i, voltage phase angle θ_i, mechanical power P_i, random noise ξ_i with noise amplitude ϵ_i, damping D_i and the coupling matrix K_{ij}, which is determined by the transmission grid topology. The operating state of a power grid is characterized by a stable fixed point of the swing equation (2). The fixed point fulfills $\omega_i^* = 0$, which is equivalent to all machines working at $f_R = 50$ Hz or $f_R = 60$ Hz. At the stable operation point the frequencies at all nodes are equal: $\omega_i = \overline{\omega}$. Deviations are only observed during system-wide failures or transiently after serious contingencies or major topology changes[11,12]. To obtain the effective equation of motion of the bulk angular velocity $\overline{\omega}$, we assume a homogeneous ratio of damping and inertia throughout the network[45], $\gamma = D_i/M_i$, as well as symmetric coupling $K_{ij} = K_{ji}$, and assume that the power is balanced $\sum_{i=1}^{N} P_i = 0$ on average[43]. Setting $M := \sum_i M_i$, the dynamics of $\overline{\omega} := \sum_{i=1}^{N} M_i \omega_i / M$ is governed by the aggregated swing equation (see also ref. [13])

$$\frac{d}{dt}\overline{\omega} = -\gamma \overline{\omega} + \overline{\epsilon}\,\overline{\xi}(t). \tag{3}$$

This aggregated swing equation no longer requires precise knowledge of the parameters of a given region, but depends on γ, the aggregated noise amplitude $\overline{\epsilon}$ and the statistics of the random noise $\overline{\xi}$, all characterizing the overall frequency dynamics; see Methods and Supplementary Note 2 for details. We note that γ integrates contributions from damper windings and primary control actions alike. Finally, both γ and $\overline{\epsilon}$ could easily change over time, for example due to connection of certain grids or day–night differences. We cover this scenario in the section on superstatistics.

$\overline{\omega}$ (and thereby the grid frequency) is not following a deterministic evolution but is influenced by stochastic effects, given by the aggregated power fluctuations $\overline{\xi}$. Hence, we characterize a given grid by the probability distribution function of the bulk angular velocity $p(\overline{\omega})$, similar to the frequency distribution plotted in Fig. 2. A wide distribution, that is, one with high standard deviation, or one with heavy tails, that is, high kurtosis, displays large deviations more often and is thereby less stable than a narrower distribution.

The central decision when modelling stochastic dynamics is how to describe ξ, which is generated from some probability distribution. Explicit choices of noise distributions are covered here and in Supplementary Notes 2 and 3 for Gaussian and non-Gaussian noise, respectively, and extended to noise drawn from a Gamma distribution[46,47] in Supplementary Note 4. Given the distribution of ξ, we then formulate and solve a Fokker–Planck equation[38] to obtain an analytical description of the distribution of $\overline{\omega}$.

The simplest noise model assumes ξ_i as independent Gaussian noise based on the often used central limit theorem. It states that the sum of independent random numbers drawn from any fixed distribution with finite variance approaches a Gaussian distribution if the sample is sufficiently large[38]. In our setting, the sum consists of all contributions to the noise by consumers, renewables, trading and so on. The Fokker–Planck equation describing the time-dependent probability density function $p(\overline{\omega}, t)$ follows then as

$$\frac{\partial p}{\partial t} = \gamma \frac{\partial}{\partial \overline{\omega}} (\overline{\omega} p) + \frac{1}{2} \sum_{i=1}^{N} \frac{\epsilon_i^2}{M^2} \frac{\partial^2 p}{\partial \overline{\omega}^2}, \tag{4}$$

which is the well known Ornstein–Uhlenbeck process[38]. The stationary distribution

$$p(\overline{\omega}) = \sqrt{\frac{\gamma M^2}{\pi \sum_{i=1}^{N} \epsilon_i^2}} \exp\left[-\overline{\omega}^2 \frac{\gamma M^2}{\sum_{i=1}^{N} \epsilon_i^2}\right], \tag{5}$$

of equation (4) characterizes the steady state of the grid as mathematically defined by $\partial p/\partial t = 0$; see ref. [38] as well as Methods and Supplementary Notes 2 and 6 for details.

Crucially, equation (5) is again a Gaussian distribution of $p(\overline{\omega})$; that is, a Gaussian distribution for the power feed-in fluctuations results in a Gaussian frequency distribution. Assuming that we know γ, ϵ_i and the total inertia M, we are able to compute the expected frequency distribution analytically. Furthermore, the Ornstein–Uhlenbeck autocorrelation exactly follows an exponential decay with characteristic time determined by the damping $\tau = 1/\gamma$.

Under which conditions do we need to include non-Gaussian effects in the stochastic modelling? When applying the central limit theorem, one explicitly assumes finite variance. However, solar and wind fluctuations are known to display heavy tails[9,24] and contribute to the fluctuations in the power grid. Hence, to describe deviations from normal distributions, including heavy tails and skewed distributions, we need to base the input noise ξ on a non-Gaussian noise-generating process[48]. This requires generalized Fokker–Planck equations; see Supplementary Note 3. These generalized equations characterize fluctuations based on noise input distributed according to, for example, a Lévy-stable law. These Lévy-stable distributions include heavy tails and skewed distributions, as often observed in nature[10], and are a reasonable fit for the frequency data; see Fig. 2. Stable distributions are characterized by a stability parameter $\alpha_S \in (0, 2]$, which determines the heavy tails, a skewness parameter β_S and a scale parameter σ_S, which is similar to the standard deviation for Gaussian distributions[36].

Inputting power fluctuations ξ drawn from a stable distribution into the stochastic equation (3) also results in grid frequency fluctuations characterized by a stable distribution, considered as the 'output' of equation (3). Between input and output distributions, only the scale parameter is modified, whereas β_S (asymmetry) and α_S (heavy-tail-ness) are preserved. In particular, the scale parameter σ_S^{in} of the input distribution changes to that of the output distribution σ_S^{out} following the map (Supplementary Notes 3 and 6)

$$\sigma_S^{\text{in}} = \frac{1}{\sqrt{2}\,M} \left[\sum_{i=1}^{N} \epsilon_i^{\alpha_S}\right]^{1/\alpha_S} \mapsto \sigma_S^{\text{out}} = \frac{\sigma_S^{\text{in}}}{(\gamma \alpha_S)^{1/\alpha_S}}. \tag{6}$$

We emphasize this remarkable and unique property of stable distributions[36] for linear models: if the input power fluctuations are distributed according to a stable distribution, the output frequency fluctuations are distributed according to the same family of distributions, with only one parameter transformed. This property holds for any linear stochastic process, including the aggregated swing equation (3). The same happens for Gaussian distributions since they constitute a subclass of stable distributions in the limit $\alpha_S \to 2$. These properties are in stark contrast to those of non-stable distributions; see Supplementary Notes 3 and 4.

What are the consequences of relation (6)? Making the output frequency distribution narrower, that is, reducing risks of extreme events, requires σ_S^{out} to be as small as possible. However, increasing the share of renewables by rebuilding the energy system is expected to increase ϵ_i. In addition, trading impacts the frequency fluctuations and thereby also contributes to the noise amplitudes (Fig. 1). However, fluctuations are efficiently reduced by increasing γ or M; see equation (6).

With the previous results, we are able to quantify the intuitive statement that larger regions have more inertia and hence narrower distributions by explicitly comparing the scale parameters (proportional to standard deviations in the case of $\alpha_S = 2$) of two different regions as follows:

$$\sigma_{S2}^{\text{out}} = \sigma_{S1}^{\text{out}} \frac{m_1}{m_2} \left(\frac{\gamma_1 N_1^{\alpha_S - 1}}{\gamma_2 N_2^{\alpha_S - 1}}\right)^{1/\alpha_S}, \tag{7}$$

assuming identical α_S and average inertia $m_\mu = M_\mu/N_\mu$, $\mu \in \{1, 2\}$. Equation (7) shows that a smaller region ($N_2 < N_1$) needs larger damping than a larger region ($\gamma_2 \geq \gamma_1$) or has a broader distribution with $\sigma_{S2}^{\text{out}} > \sigma_{S1}^{\text{out}}$, that is, a higher risk of large deviations from the stable operational range. The scaling is given by $\sigma_S \sim N^{(\alpha_S - 1)/\alpha_S}$, where the simple square-root law is recovered only in the case of Gaussian distributions ($\alpha_S = 2$). Also, it reveals that decreasing inertia proportionally increases the scale parameter.

Furthermore, we estimate the order of magnitude of the expected noise amplitude

$$\epsilon = \sigma_S^{\text{out}} m (\alpha_S \gamma N^{\alpha_S - 1})^{1/\alpha_S} \tag{8}$$

by computing the scaling from (6) for typical noise contributions of the order of $\epsilon_i = \epsilon$. Based on pure frequency measurements, every quantity is available for each synchronous region. We estimate σ_S^{out} and α_S from the histogram data. We assume that the number of nodes N is directly proportional to the total electricity production of a region per year[49,50]. Since a process driven by stable noise has no defined autocorrelation function[36], we approximate its autocorrelation with the Ornstein–Uhlenbeck process and thereby derive an estimate for γ. With these estimates and equation (8) we plot the noise amplitudes for different regions in Fig. 5. The estimated noise amplitude tends to increase with increasing share of intermittent renewable generation (wind and solar) in a given region. Nevertheless, this relationship is not very strict, and frequency disturbances at trading intervals (see Fig. 1) demonstrate that, at least today, trading and demand fluctuations are contributing substantially to frequency fluctuations.
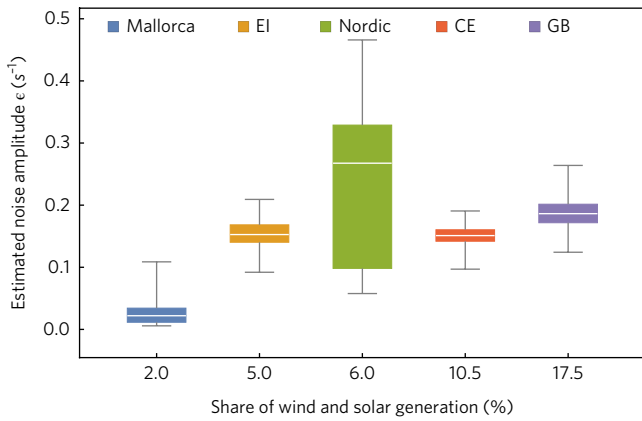
Fig. 5 | Noise amplitudes for European and American grids. The noise amplitude tends to increase with the shares of intermittent renewables. The ϵ for each grid is calculated assuming that it is identical at each node $\epsilon_i = \epsilon$ and assuming homogeneous inertia. The power production is normalized with respect to EI generation for the CE, Mallorcan, Nordic and GB ENTSO-E grids. Frequency data of all regions and equation (8) are used to compute ϵ, which we expect to be similar in all regions, providing a self-consistency check of our theory. The box plot is obtained by using different dampings, standard deviation estimates and so on for each day of multiple years. The data for the Nordic grid have large uncertainty due to the two different correlation timescales. See Supplementary Note 1 for details on the data.

Superstatistics. Instead of modelling the underlying stochastic process as non-Gaussian, we may interpret the observed statistics as a superposition of multiple Gaussians, leading to *superstatistics*, explaining heavy tails and skewness[51,52].

For our superstatistical approach we use equation (3) with Gaussian noise $\overline{\xi}$,

$$\frac{\mathrm{d}}{\mathrm{d}t}\overline{\omega} = -\gamma\overline{\omega} + \overline{\epsilon}\,\overline{\xi}(t), \qquad (9)$$

which yields a Gaussian distribution; see equation (5).

What changes when γ is no longer constant over time? Both control actions and physical damping contribute to γ and change over time when certain power plants are connected and others are shut down. Similarly, the $\overline{\epsilon}$ of the system depends on which consumers are currently active, whether it is day or night, which renewables are connected and more. Hence, it is appropriate to replace our static parameters γ and $\overline{\epsilon}$ by dynamical parameters that change over time with a typical timescale T. When applying superstatistics, we assume that T is large compared with the intrinsic timescale of the system, which is given by the autocorrelation timescale, namely $T \gg \tau = 1 / \gamma$. Then, the stochastic process finds an equilibrium with an approximately Gaussian distribution determined by the current noise and damping. When these parameters change, the frequency distribution becomes a Gaussian distribution with different standard deviation. In Fig. 6a we demonstrate how just a few Gaussian distributions with different standard deviations give rise to an excess kurtosis, and in Supplementary Note 5 we show how two Gaussian distributions with shifted means result in a skewed distribution.

We extract the long timescale T from the data and compare it with the intrinsic short timescale of the system. The short timescale $\tau = 1/\gamma$ is based on the exponential decay of the autocorrelation of the time series of $\overline{\omega}$, yielding a range of $\tau \approx 200$–$550\,\mathrm{s}$ for all grids. T is governed by the idea that the superstatistical ensemble has heavier tails than a normal distribution, but that for a given typical T an equilibrium distribution emerges that is approximately Gaussian. Given a time series $x(t)$ with mean $\overline{x}$, we compute the local kurtosis $\kappa(\Delta t)$ for different time intervals Δt and choose T by $\kappa(\Delta t = T) = 3$ (ref. [51]). Similarly, we compute the time for which the average skewness is zero to extract the long timescale for the GB or EI grids; see Methods and Supplementary Note 5 for details and Fig. 6 for an example for Japan.

All synchronous regions return large but different T. We determine the long timescales to be of the order of $T \approx 1$–$5\,\mathrm{h}$ with small values in Mallorca and the EI and large values in CE and Japan, hinting at distinct underlying mechanisms for damping and noise change in each region. Compared with the intrinsic $\tau \sim 200$–$500\,\mathrm{s}$, T is larger by at least one order of magnitude. Hence, the superstatistical approach is justified; that is, it is valid to interpret the heavy tails as a result of superimposing Gaussians.

Finally, we perform another consistency check of the superstatistical approach and extract the distribution of the effective friction
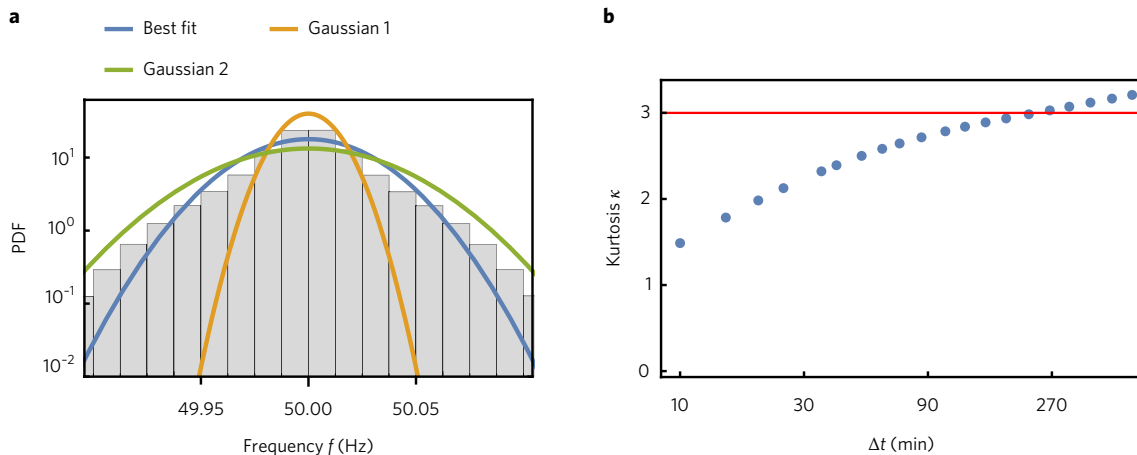

Fig. 6 | Superimposed Gaussian distributions leading to heavy tails. a, When the stochastic process follows two different Gaussian distributions (orange and green) and the data are aggregated (grey histogram), the result is a heavy-tailed distribution that is not Gaussian. Consequently, Gaussian fits (blue curve) tend to underestimate its tails. Assuming such a structure for the real frequency measurements, the frequency recordings are split into trajectories of length Δt each and the kurtosis is computed. **b**, The average kurtosis of the Japanese 60 Hz dataset is plotted as a function of the length of Δt. For very small Δt the distribution has lighter tails than a Gaussian, while using the full dataset or large Δt leads to the earlier observed heavy tails. T, during which the distribution changes, is determined as $\kappa(\Delta t = T) = 3$.
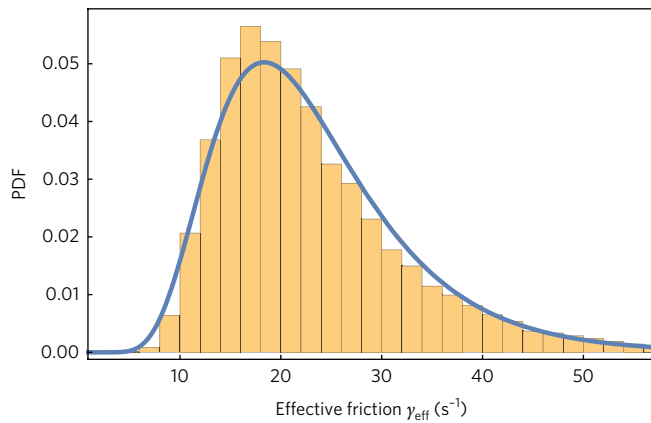
Fig. 7 | Self-consistency test of superstatistics. The histogram of γ_{eff} based on the Japanese 60 Hz frequency measurements, which is well described by a log-normal distribution. Such a distribution of γ_{eff} directly leads to q-Gaussian distributions of the aggregated data; see Supplementary Note 5. Other datasets are also approximated by log-normal distributions; see Supplementary Note 5.

γ_{eff} (ref. [51]); see Methods. Based on general results on superstatistics, we expect the effective friction to follow a χ^2, inverse χ^2 or log-normal distribution[53,54], which then leads to an approximate q-Gaussian distribution of the frequency; see Supplementary Note 5 for a derivation. In the case of the Japanese 60 Hz region the distribution of γ_{eff} is well described by a log-normal distribution, again supporting the superstatistical approach; see Fig. 7.

Discussion

In summary, we have analysed power grid frequency fluctuations by applying analytical stochastic methods to time series of different synchronous regions across continents including North America, Japan and different European regions. Based on bulk frequency measurements, we have identified trading as a substantial source of fluctuations (Figs. 1 and 3). Although frequency fluctuations and power uncertainty are often modelled as Gaussian distributions[16,18–21], we pinned down and quantified substantial deviations from a Gaussian form, including heavy tails and skewed distributions (Fig. 2).

Obtaining an analytical description of a complex system allows deeper insight into it. Hence, condensing the analysis of frequency fluctuations in power grids via a second-order nonlinear dynamics, the swing equation, and neglecting spatial correlations, we derived (generalized) Fokker–Planck equations for $\overline{\omega}$. We obtained precise predictions on how power fluctuations impact the distribution of fluctuations of the grid frequency. Furthermore, our approach identifies, besides grid size, an increasing effective damping and inertia as a controlling factor for reducing fluctuation-induced risks. By incorporating smart grid control mechanisms[4] or increasing generator droop control[11], modifying effective damping may therefore reliably reduce the likelihood of large fluctuations in power grids[55]. Finally, our analytical theory is able to compare different sized grids, and predict fluctuations based on the size and inertia of the grid (equation (7)). Crucially, our mathematical framework goes beyond the simple $N^{-1/2}$ scaling of Gaussian noise.

The results offer two approaches to model power grids under uncertainty. First, an optimization could include the non-Gaussian nature of the distribution by incorporating non-Gaussian noise, for example in the form of Lévy-stable noise. Alternatively, we have demonstrated that the distributions are also well explained by a

superstatistics approach, where the non-Gaussian nature of the distributions arises by superimposing different Gaussian distributions. Especially when modelling shorter timescales of 1 h or less, a Gaussian approach is supported by our results. Studies aiming to cover timescales of full months or years, however, have to account for the changing mean and variance of the assumed Gaussian distribution, or explicitly model non-Gaussian distributions, going beyond current Gaussian approaches[16,18–21].

The findings reported above have a number of implications for the operation and design of current and future energy systems. First, as trading induces large frequency fluctuations, designing new electricity markets and limiting frequency fluctuations are highly interlinked, especially when considering the implementation of smart grid concepts[4,21]. Second, knowing the temporal correlation structure of fluctuations helps predict increasing and decreasing likelihoods of large-amplitude events, thereby enabling mitigation strategies to be applied on timescales that make them most efficient. Finally, deriving the scaling of fluctuations as a function of grid parameters, especially the grid size, should be very useful when setting up isolated grids, for example microgrids with a specified frequency quality, as damping and control needs can easily be estimated by the approach introduced above. This may also be of use for larger synchronous regions when facing a decreasing M.

Moreover, applying similar stochastic methods to power grids also raises a range of additional questions. How does correlated noise impact the frequency statistics? Does the predicted scaling of fluctuations with the grid size hold for a larger collection of independent power grids and in particular very small islands or microgrids? Can we disentangle damping and primary control to explain the differences of long timescales among different regions? These questions require further careful data analysis in future work, involving substantially more data on microgrids, work that could inspire further collaboration including a range of academic fields as well as public institutions and industry.

Methods

Moments of the frequency distributions. Deviations from Gaussian distributions as observed in Fig. 2 are quantified in a model-independent way using moments of the frequency distribution: given N_M measurements of a discrete stochastic variable f, for example the grid frequency, as $f_1, f_2, \ldots, f_{N_M}$, its nth moment is defined as

$$\mu_n := \frac{1}{N_M} \sum_{i=1}^{N_M} f_i^n. \tag{10}$$

The first moment of a distribution is the mean $\mu_1 \equiv \mu$. Instead of the second moment, the centralized second moment, that is, the variance, is more commonly used. It is defined as

$$\sigma^2 := \frac{1}{N_M} \sum_{i=1}^{N_M} \left(f_i - \mu\right)^2. \tag{11}$$

Finally, we use the normalized third and fourth moments, β and κ, respectively, which are defined as

$$\beta := \frac{1}{N_M} \sum_{i=1}^{N_M} \left(\frac{f_i - \mu}{\sigma}\right)^3, \tag{12}$$

$$\kappa := \frac{1}{N_M} \sum_{i=1}^{N_M} \left(\frac{f_i - \mu}{\sigma}\right)^4. \tag{13}$$

A Gaussian distribution is symmetric and hence β is equal to zero. A non-zero skewness implies a distribution that is not symmetric around the mean but is more pronounced in one direction. The kurtosis meanwhile quantifies the extremity of the tails. A Gaussian distribution has $\kappa^{Gauss} = 3$, while a higher value indicates an increased likelihood of large deviations. For instance, the CE grid displays a kurtosis of $\kappa^{CE} = 4.0 \pm 0.1$.

Normally distributed noise. For equation (4) we took the sum over multiple noise realizations that follow a normal distribution. Let ξ_i be random variables following a normal distribution, that is,

$$\xi_i \sim N(0, 1), \qquad (14)$$

where $N(0, 1)$ denotes a normal distribution with mean 0 and standard deviation 1. Then, the sum of identically and independently distributed random variables ξ_i given as

$$\overline{\epsilon}\overline{\xi} := \sum_{i=1}^{N} \epsilon_i \xi_i \qquad (15)$$

is distributed like a single normal distribution[36]

$$\overline{\epsilon}\overline{\xi} \sim N\left(0, \sqrt{\sum_{i=1}^{N} \epsilon_i^2}\right). \qquad (16)$$

Superstatistics. In Figs. 6 and 7 we extract the local kurtosis and effective damping from the time series as follows. Let $x(t)$ be a time series of random measurements with a mean $\overline{x}$. To test whether $x(t)$ is aggregated by drawing from multiple distributions, we compute the local kurtosis as

$$\kappa(\Delta t) = \frac{1}{t_{max} - \Delta t} \int_0^{t_{max} - \Delta t} \frac{\langle (x - \overline{x})^4 \rangle_{t_0, \Delta t}}{\langle (x - \overline{x})^2 \rangle_{t_0, \Delta t}^2} dt_0, \qquad (17)$$

where $\langle \cdots \rangle_{t_0, \Delta t} = \int_{t_0}^{t_0 + \Delta t} \cdots dt$. We do so for several values of Δt and choose T such that $\kappa(\Delta t = T) = 3$; that is, averaging over T, there is no excess kurtosis and locally the variable x is subject to Gaussian noise.

γ_{eff}, which is changing over time, is then computed as

$$\gamma_{eff}(t_0) = \frac{1}{\langle x^2 \rangle_{t_0, T} - \langle x \rangle_{t_0, T}^2}. \qquad (18)$$

Following ref. [51] we expect γ_{eff} to follow a log-normal or alternatively a χ^2 or inverse χ^2 distribution, as these lead to q-Gaussian distributions of x; see Supplementary Note 5.

Data availability. Frequency recordings are publicly available at the respective references for the CE, GB, Nordic and Japanese regions[29–31,33,34]. Frequency data for Mallorca[32] were provided by Eder Batista Tchawou Tchuisseu. Data for the EI (ref. [35]) were provided by Micah Till. All data that support the results presented in the figures of this study are available from the authors upon reasonable request.

References

1. *Adoption of the Paris Agreement* FCCC/CP/2015/L.9/Rev.1 (UNFCCC, 2015).
2. IPCC *Climate Change 2014: Impacts, Adaptation and Vulnerability* (eds Field, C. B. et al.) Part B (Cambridge University Press, Cambridge, 2014).
3. Jacobson, M. Z. & Delucchi, M. A. Providing all global energy with wind, water, and solar power, Part I: Technologies, energy resources, quantities and areas of infrastructure, and materials. *Energy Policy* **39**, 1154–1169 (2011).
4. Schäfer, B., Matthiae, M., Timme, M. & Witthaut, D. Decentral smart grid control. *New J. Phys.* **17**, 015002 (2015).
5. Turner, J. A. A realizable renewable energy future. *Science* **285**, 687–689 (1999).
6. Boyle, G. *Renewable Energy* (Oxford University Press, Oxford, 2004).
7. Ueckerdt, F., Brecha, R. & Luderer, G. Analyzing major challenges of wind and solar variability in power systems. *Renewable Energy* **81**, 1–10 (2015).
8. Heide, D. et al. Seasonal optimal mix of wind and solar power in a future, highly renewable Europe. *Renewable Energy* **35**, 2483–2489 (2010).
9. Milan, P., Wächter, M. & Peinke, J. Turbulent character of wind energy. *Phys. Rev. Lett.* **110**, 138701 (2013).
10. Peinke, J. et al. in *Advances in Solid State Physics* 363–373 (Springer, Berlin, 2004).
11. Machowski, J., Bialek, J. & Bumby, J. *Power System Dynamics: Stability and Control* (Wiley, Chichester, 2011).
12. Kundur, P., Balu, N. J. & Lauby, M. G. *Power System Stability and Control* 7 (McGraw-Hill, New York, 1994).
13. Ulbig, A., Borsche, T. S. & Andersson, G. Impact of low rotational inertia on power system stability and operation. *IFAC Proc. Vol.* **47**, 7290–7297 (2014).
14. Delille, G., Francois, B. & Malarange, G. Dynamic frequency control support by energy storage to reduce the impact of wind and solar generation on isolated power system's inertia. *IEEE Trans. Sustain. Energy* **3**, 931–939 (2012).
15. Doherty, R. et al. An assessment of the impact of wind generation on system frequency control. *IEEE Trans. Power Syst.* **25**, 452–460 (2010).
16. Wood, A. J. & Wollenberg, B. F. *Power Generation, Operation, and Control* (Wiley, 2012).
17. National Academies of Sciences Engineering and Medicine. *The Power of Change: Innovation for Development and Deployment of Increasingly Clean Electric Power Technologies* (National Academies Press, Washington DC, 2016).
18. Jin, Y. & Branke, J. Evolutionary optimization in uncertain environments—a survey. *IEEE Trans. Evol. Comput.* **9**, 303–317 (2005).
19. Zhang, H. & Li, P. Probabilistic analysis for optimal power flow under uncertainty. *IET Gener. Transm. Distrib.* **4**, 553–561 (2010).
20. Schäfer, B. et al. Escape routes, weak links, and desynchronization in fluctuation-driven networks. *Phys. Rev. E* **95**, 060203 (2017).
21. Fang, X., Misra, S., Xue, G. & Yang, D. Smart Grids—the new and improved power grid: a survey. *IEEE Commun. Surv. Tutor.* **14**, 944–980 (2012).
22. Kashima, K., Aoyama, H. & Ohta, Y. Modeling and linearization of systems under heavy-tailed stochastic noise with application to renewable energy assessment. In *2015 54th IEEE Conference on Decision and Control (CDC)* 1852–1857 (IEEE, New York, 2015).
23. Mühlpfordt, T., Faulwasser, T. & Hagenmeyer, V. Solving stochastic AC power flow via polynomial chaos expansion. In *2016 IEEE Conference on Control Applications (CCA)* 70–76 (IEEE, New York, 2016).
24. Anvari, M. et al. Short term fluctuations of wind and solar power systems. *New J. Phys.* **18**, 063027 (2016).
25. Schmietendorf, K., Peinke, J. & Kamps, O. On the stability and quality of power grids subjected to intermittent feed-in. Preprint at https://arxiv.org/abs/1611.08235 (2016).
26. Li, X., Hui, D. & Lai, X. Battery energy storage station (BESS)-based smoothing control of photovoltaic (PV) and wind power generation fluctuations. *IEEE Trans. Sust. Energy* **4**, 464–473 (2013).
27. Lauby, M. G., Bian, J. J., Ekisheva, S. & Varghese, M. Frequency response assessment of ERCOT and Québec interconnections. In *2014 North American Power Symposium (NAPS)* 1–5 (IEEE, New York, 2014).
28. Lasseter, R. H. & Paigi, P. Microgrid: a conceptual solution. In *2004 IEEE 35th Annual Power Electronics Specialists Conference (PESC)* vol. 6, 4285–4290 (IEEE, New York, 2004).
29. *Network Frequency (2014–2016)* (RTE, 2017); https://clients.rte-france.com/lang/an/visiteurs/vie/vie_frequence.jsp.
30. *ENTSO-E Netzfrequenz* (50Hertz, 2010–2016); http://www.50hertz.com/de/Maerkte/Regelenergie/Regelenergie-Downloadbereich.
31. *Frequency Measurement Data* (Fingrid, 2015–2016); http://www.fingrid.fi/en/powersystem/Power%20system%20management/Maintaining%20of%20balance%20between%20electricity%20consumption%20and%20production/Frequency%20measurement%20data/Pages/default.aspx.
32. Tchuisseu, E. B., Gomila, D., Brunner, D. & Colet, P. Effects of dynamic-demand-control appliances on the power grid frequency. Preprint at https://arxiv.org/abs/1704.01638 (2017).
33. *Frequency Data* (National Grid, 2014–2016); http://www2.nationalgrid.com/Enhanced-Frequency-Response.aspx.
34. *Japanese Grid Frequency* (OCCTO, 2016); http://occtonet.occto.or.jp/public/dfw/RP11/OCCTO/SD/LOGIN_login#.
35. *FNET/GridEye* (Power Information Technology Lab, University of Tennessee, Knoxville and Oak Ridge National Laboratory, 2014); http://powerit.utk.edu/fnet.html.
36. Samorodnitsky, G. & Taqqu, M. S. in *Stable Non-Gaussian Processs: Stochastic Models with Infinite Variance* (Chapman and Hall, New York, 1994).
37. Tsallis, C. Nonadditive entropy and nonextensive statistical mechanics—an overview after 20 years. *Braz. J. Phys.* **39**, 337–356 (2009).
38. Gardiner, C. W. *Handbook of Stochastic Methods*. 3rd edn (Springer, Berlin, 1985).
39. Filatrella, G., Nielsen, A. H. & Pedersen, N. F. Analysis of a power grid using a Kuramoto-like model. *Eur. Phys. J. B* **61**, 485–491 (2008).
40. Rohden, M., Sorge, A., Timme, M. & Witthaut, D. Self-organized synchronization in decentralized power grids. *Phys. Rev. Lett.* **109**, 064101 (2012).
41. Dörfler, F., Chertkov, M. & Bullo, F. Synchronization in complex oscillator networks and smart grids. *Proc. Natl Acad. Sci. USA* **110**, 2005–2010 (2013).
42. Motter, A. E., Myers, S. A., Anghel, M. & Nishikawa, T. Spontaneous synchrony in power-grid networks. *Nat. Phys.* **9**, 191–197 (2013).
43. Manik, D. et al. Supply networks: instabilities without overload. *Eur. Phys. J. Spec. Top.* **223**, 2527–2547 (2014).
44. Dewenter, T. & Hartmann, A. K. Large-deviation properties of resilience of power grids. *New J. Phys.* **17**, 015005 (2015).

45. Weixelbraun, M., Renner, H., Schmaranz, R. & Marketz, M. Dynamic simulation of a 110-kV-network during grid restoration and in islanded operation. In *20th International Conference and Exhibition on Electricity Distribution-Part 1, 2009* 1–4 (IET, Stevenage, 2009).

46. Carpaneto, E. & Chicco, G. Probabilistic characterisation of the aggregated residential load patterns. *IET Gener. Transm. Distrib.* **2**, 373–382 (2008).

47. Soubdhan, T., Emilion, R. & Calif, R. Classification of daily solar radiation distributions using a mixture of Dirichlet distributions. *Sol. Energy* **83**, 1056–1063 (2009).

48. Denisov, S., Horsthemke, W. & Hänggi, P. Generalized Fokker–Planck equation: derivation and exact solutions. *Eur. Phys. J. B* **68**, 567–575 (2009).

49. *Monthly Production for a Specific Year for 2015* (ENTSO-E, 2016); https://www.entsoe.eu/db-query/production/monthly-production-for-a-specific-year.

50. *Eia-411: Coordinated Bulk Power Supply and Demand Program Report* (US Department of Energy, 2016); https://www.eia.gov/electricity/data/eia411/.

51. Beck, C. & Cohen, E. G. D. Superstatistics. *Physica A* **322**, 267–275 (2003).

52. Chechkin, A. V., Seno, F., Metzler, R. & Sokolov, I. M. Brownian yet non-gaussian diffusion: from superstatistics to subordination of diffusing diffusivities. *Phys. Rev. X* **7**, 021002 (2017).

53. Clark, P. K. A subordinated stochastic process model with finite variance for speculative prices. *Econometrica* **41**, 135–155 (1973).

54. Castaing, B., Gagne, Y. & Hopfinger, E. Velocity probability density functions of high Reynolds number turbulence. *Physica D* **46**, 177–200 (1990).

55. Schöll, E. & Schuster, H. G. *Handbook of Chaos Control* (2008).

Author contributions

B.S., D.W. and M.T. conceived and designed the research. B.S. acquired the data, performed the data analysis and formulated stochastic predictions. All authors contributed to discussing the results and writing the manuscript.

Competing interests

The authors declare no competing financial interests.

Additional information

Supplementary information is available for this paper at https://doi.org/10.1038/s41560-017-0058-z.

Reprints and permissions information is available at www.nature.com/reprints.

Correspondence and requests for materials should be addressed to B.S.

Publisher's note: Springer Nature remains neutral with regard to jurisdictional claims in published maps and institutional affiliations.